Electronic Supplementary Material (ESI) for Journal of Materials Chemistry A.
This journal is © The Royal Society of Chemistry 2021

Supplementary Information

Overcoming Carrier Transport Limitation in Ruddlesden−Popper Perovskite Films by Lamellar Nickel Oxide Substrate

Jianghu Liang[a], Zhanfei Zhang[a], Yiting Zheng[a], Xueyun Wu[a], Jianli Wang[a], Zhuang Zhou[a], Yajuan Yang[a], Ying Huang[a], Zhenhua Chen[b], and Chun-Chao Chen[a]*

[a]School of Materials Science and Engineering, Shanghai Jiao Tong University, Shanghai 200240, P. R. China

[b]Shanghai Synchrotron Radiation Facility (SSRF), Shanghai Advanced Research Institute, Chinese Academy of Sciences, Shanghai 201800, P. R. China

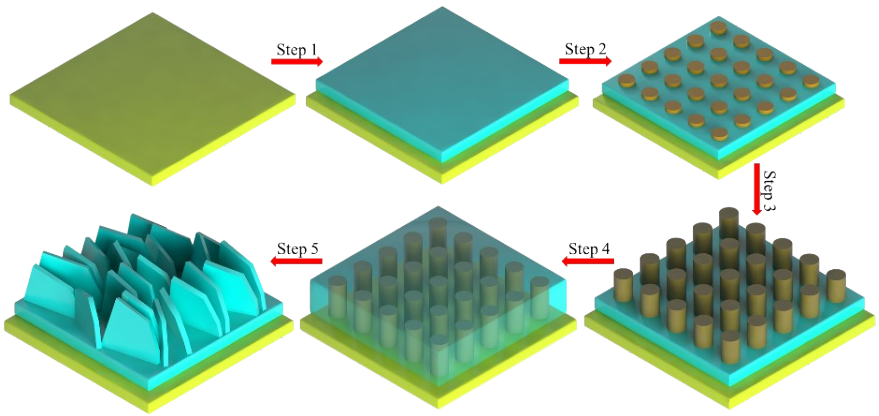

Figure S1 Schematic diagram of the fabrication process of lamellar-NiO_x.

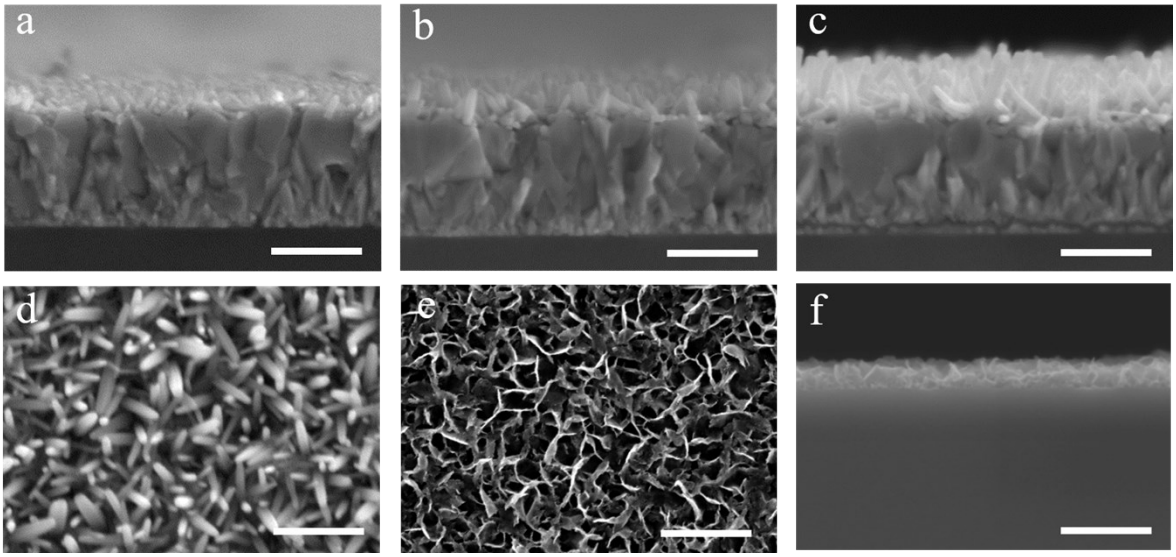

Figure S2 Cross-sectional SEM images of ZnO nanorods template with three length, (a) 100 nm, (b) 200 nm, (c) 300 nm. (d) surface SEM image of ZnO nanorods template. Surface SEM image of 130 nm long lamellar-NiO_x on (e) single crystal silicon substrate and (f) its cross-sectional SEM image. Scale bar: 500 nm.

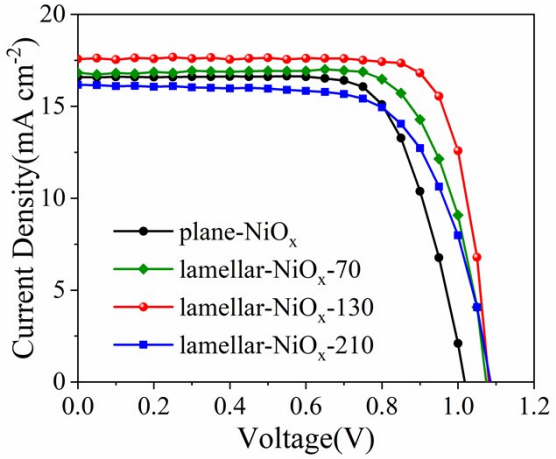

Figure S3 J-V curves of $FPEA_2MA_3Pb_4I_{13}$ on various NiO_x substrates.

Table S1 Photovoltaic parameters of $FPEA_2MA_3Pb_4I_{13}$ on various NiO_x substrates.

Substrate	V_{oc}(V)	J_{sc} (mA cm^{-2})	FF	PCE(%)
plane-NiO_x	1.02	16.6	0.72	12.3
lamellar-NiO_x-70	1.07	16.8	0.74	13.3
lamellar-NiO_x-130	1.08	17.6	0.80	15.2
lamellar-NiO_x-210	1.09	16.1	0.68	12.0

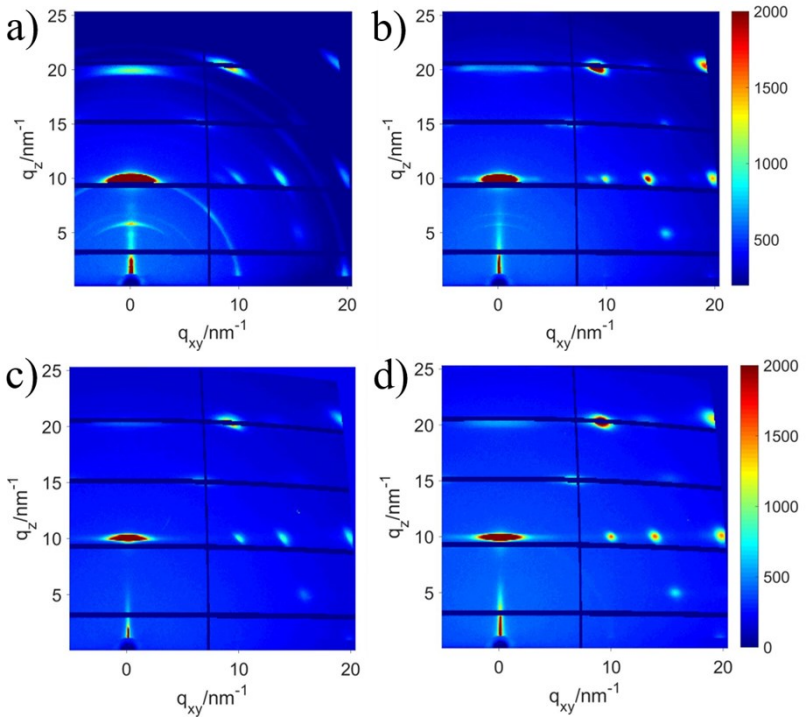

Figure S4 GIWAXS patterns of (a) BA-plane, (b) BA-lamellar, (c) PEA-plane, (d) PEA-lamellar.

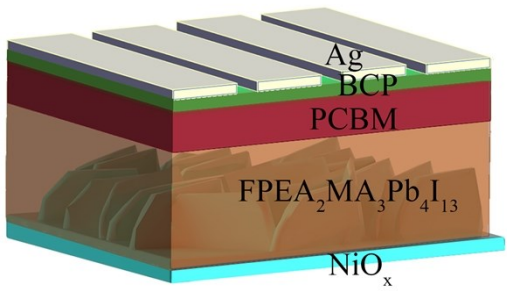

Figure S5 Device structure of FPEA-lamellar.

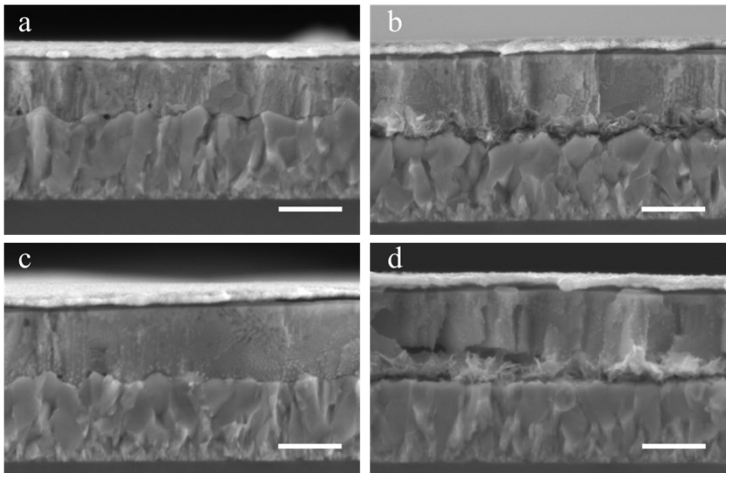

Figure S6 Cross-sectional SEM images of (a) BA-plane, (b) BA-lamellar, (c) PEA-plane, and (d) PEA-lamellar. Scale bar: 500 nm.

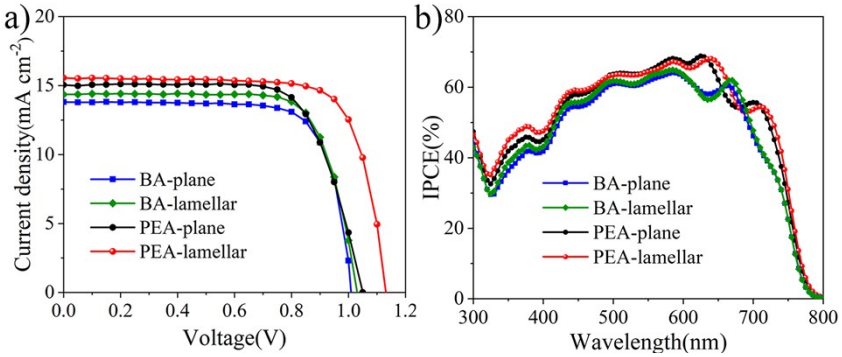

Figure S7 (a) J-V curves of BA-plane, BA-lamellar, PEA-plane, and PEA-lamellar and (b) their EQE spectra.

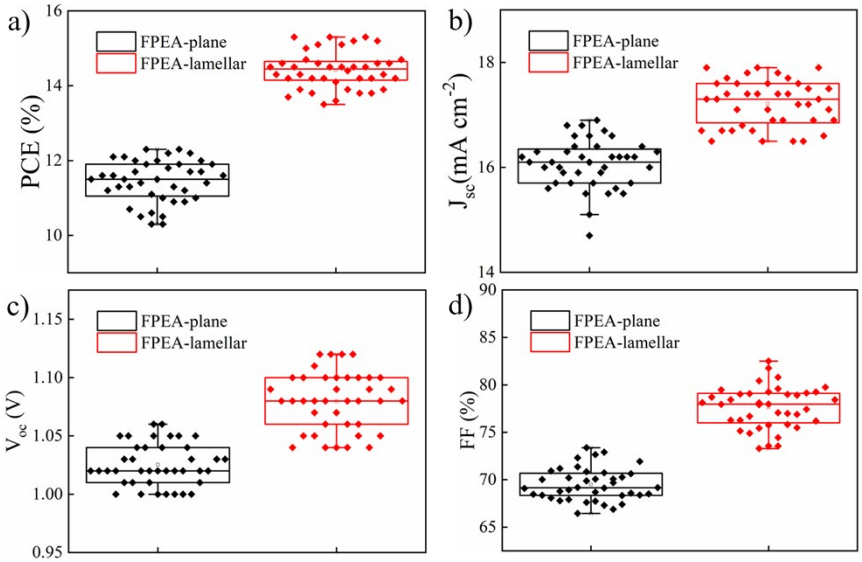

Figure S8 Statistics photovoltaic parameters of FPEA-plane and PFEA-lamellar. (a) PCE, (b) J_{sc}, (c) V_{oc}, (d) FF.

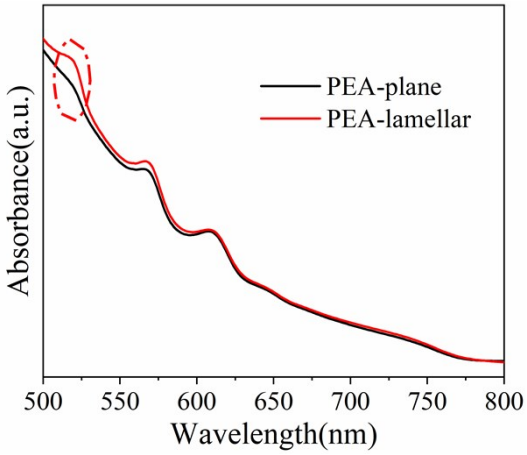

Figure S9 UV-vis absorption spectra of PEA-plane and PEA-lamellar.

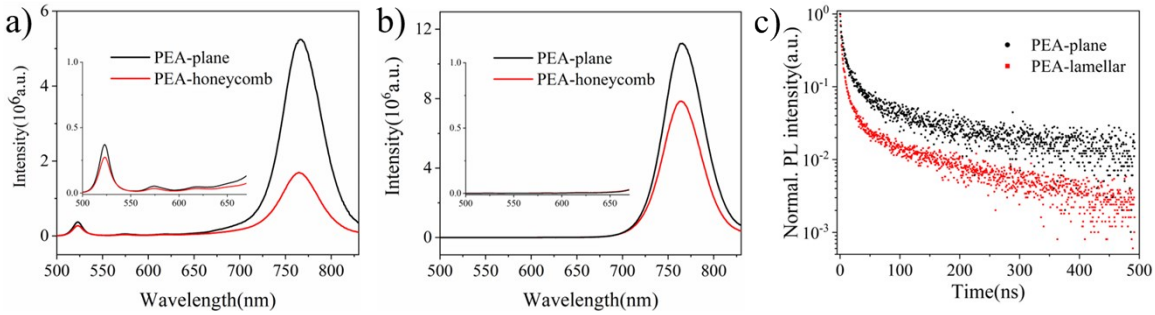

Figure S10 PL spectra of PEA-plane and PEA-lamellar under (a) back side excitation, (b) front side excitation. (c) TRPL of PEA-plane and PEA-lamellar under back side excitation.

Table S2 Fitting parameters of TRPL decay curves of 2D perovskite films. Fitting function: $Y=A_1\exp(-t/\tau_1) + A_2\exp(-t/\tau_2) + y_0$, $\tau_{ave}=(A_1*\tau_1^2+A_2*\tau_2^2)/(A_1*\tau_1+A_2*\tau_2)$[1, 2].

Sample	τ_1(ns)	A_1	τ_2(ns)	A_2	τ_{ave}(ns)
BA-plane	2.1	81%	28.3	19%	22.1
BA-lamellar	1.6	90%	27.6	10%	18.9
PEA-plane	3.4	80%	42.0	20%	32.4
PEA-lamellar	2.2	87%	24.1	13%	15.8
FPEA-plane	1.4	84%	67.3	16%	60.7
FPEA-lamellar	1.1	88%	39.8	12%	33.3

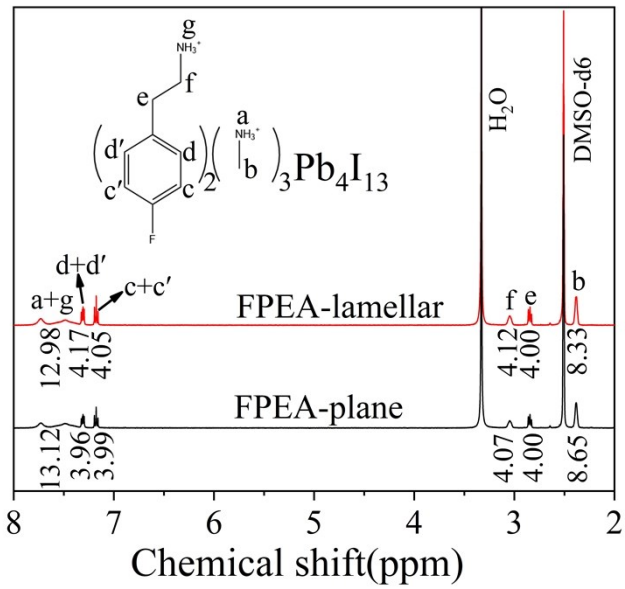

Figure S11 ^{1}H NMR spectra of FPEA-plane and FPEA-lamellar

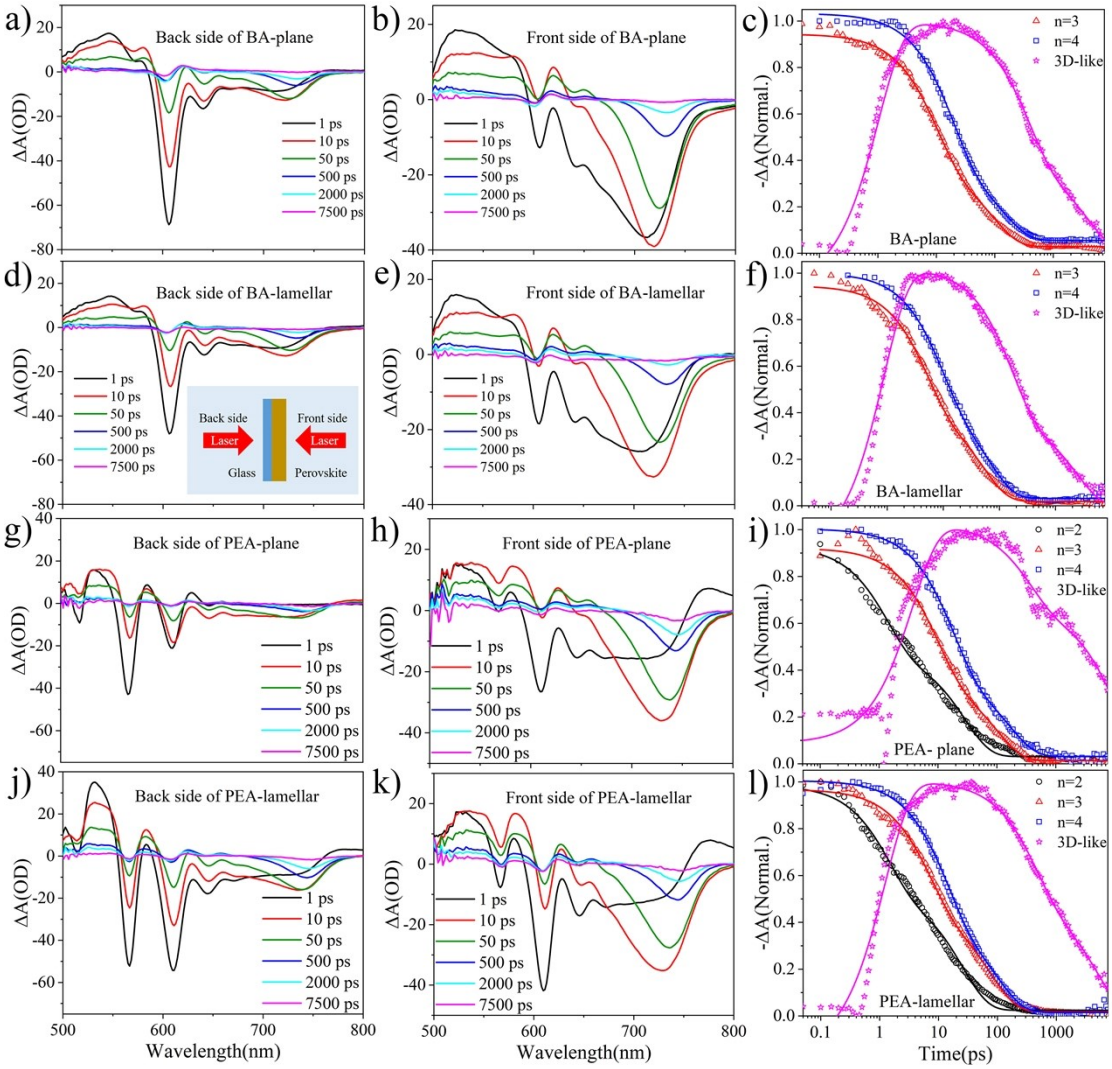

Figure S12 Representative TA spectra of BA and PEA based 2D perovskite films under (a, d, g, j) back side excitation and (b, e, h, k) front side excitation, and its corresponding kinetic curves (c, f, i, l) under back side excitation. The solid lines are fitting curves of TA kinetics.

Table S3 Fitting parameters of TA kinetics of FPEA-lamellar and FPEA-plane. Fitting function: $\Delta A(t) = A_1\exp(-t/\tau_1) + A_2\exp(-t/\tau_2) - C_1\exp(-t/\tau_{et})^3$.

Phases of FPEA	τ_1(ps)(lamellar/plane)	τ_2(ps) (lamellar/plane)	τ_{et}(ps) (lamellar/plane)
n=2	0.8±0.05/1.0±0.07	31.6±1.53/31.1±1.70	/
n=3	3.2±0.10/6.1±0.24	56.1±2.02/82.8±5.05	/
n=4	5.1±0.21/8.0±0.34	56.0±3.75/83.4±5.54	/
3D-like	196.1±21.69/ 282.1±51.18	3962.2±496.09/ 7617.9±1527.09	1.1±0.05/2.4±0.13

Table S4 Fitting parameters of TA kinetics of BA-lamellar and BA-plane. Fitting function: $\Delta A(t) = A_1\exp(-t/\tau_1) + A_2\exp(-t/\tau_2) - C_1\exp(-t/\tau_{et})$.

Phases of BA	τ_1(ps)(lamellar/plane)	τ_2(ps) (lamellar/plane)	τ_{et}(ps) (lamellar/plane)
n=3	4.8±0.24/9.7±0.32	51.2±2.91/93.0±4.86	/
n=4	8.7±0.33/18.3±0.70	67.2±2.70/139.6±9.72	/
3D-like	162.8±13.18/ 366.3±33.78	2400.7±319.90/ 4062.8±646.65	0.9±0.03/1.0±0.04

Table S5 Fitting parameters of TA kinetics of PEA-lamellar and PEA-plane. Fitting function: $\Delta A(t) = A_1\exp(-t/\tau_1) + A_2\exp(-t/\tau_2) - C_1\exp(-t/\tau_{et})$.

Phases of PEA	τ_1(ps)(lamellar/plane)	τ_2(ps) (lamellar/plane)	τ_{et}(ps) (lamellar/plane)
n=2	1.4±0.08/1.3±0.10	25.6±1.07/28.3±1.46	/
n=3	6.8±0.27/9.4±0.69	76.9±3.24/99.2±10.33	/
n=4	13.1±0.50/17.2±0.58	101.6±5.33/165.0±8.68	/
3D-like	425.3±59.43/ 352.1±79.37	5018.4±825.70/ 10649.9±2053.40	1.3±0.05/3.8±0.25

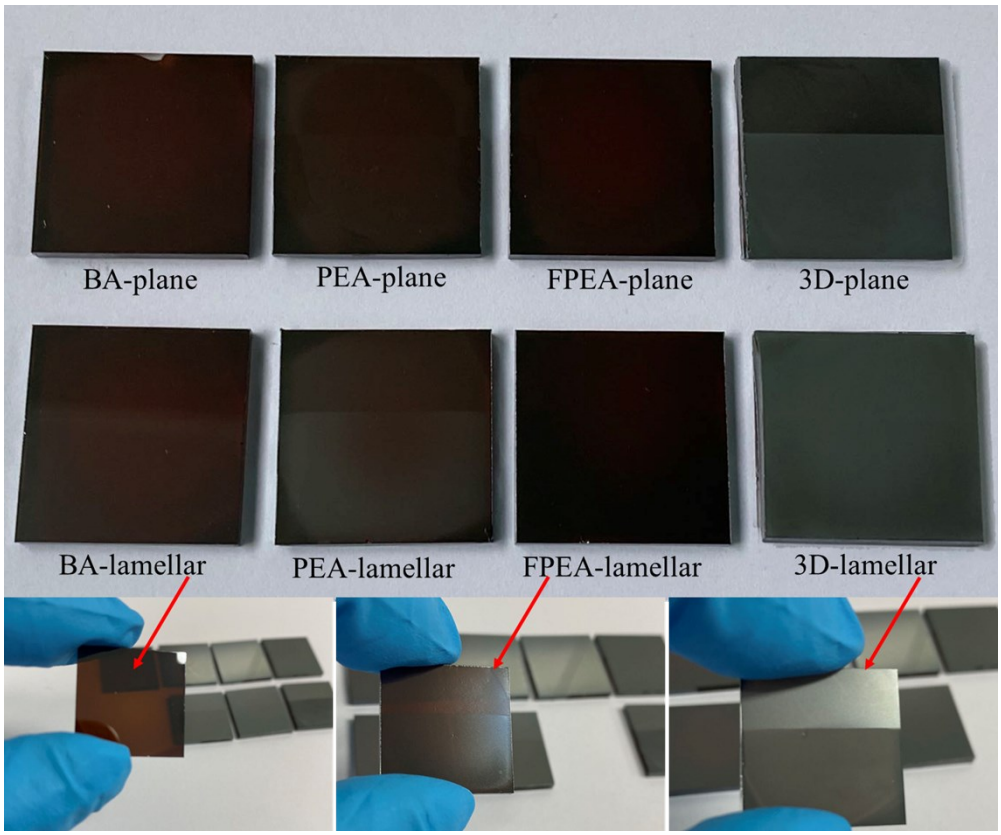

Figure S13 Photographic images of 2D and 3D perovskite films on lamellar-NiO_x and plane-NiO_x substrate. The side length of FTO glass is 2 cm.

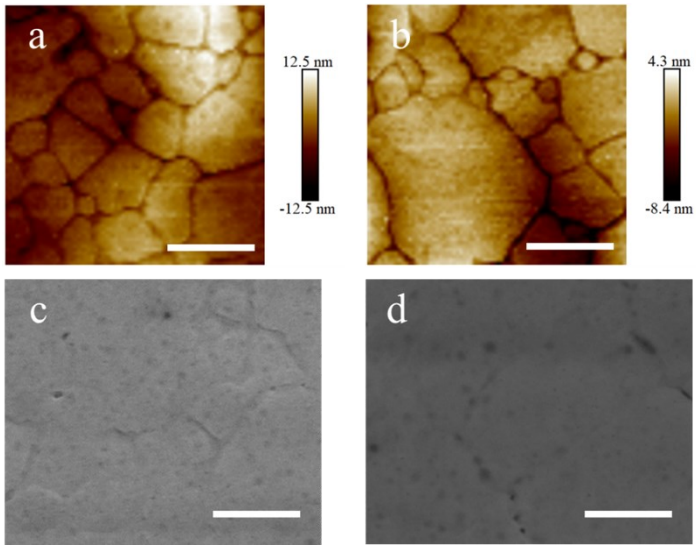

Figure S14 AFM (height sensor) and SEM images of (a), (c) FPEA-plane, and (b), (d) FPEA-lamellar. Scale bar: 500 nm.

Table S6 Calculated lattice parameters of R_2PbI_4 (R=BA, PEA, FPEA).

Lattice parameters	BA	PEA	FPEA
a(Å)	8.54	8.70	8.60
b(Å)	9.08	9.07	9.10
c(Å)	13.28	16.61	16.15
α(°)	93.34	92.88	90.50
β(°)	84.03	86.72	95.19
γ(°)	90.69	90.06	90.01
Pb-I-Pb angle(°)	152.86	159.41	158.40
Formation energy(eV)	-2.92	-.2.27	-2.36

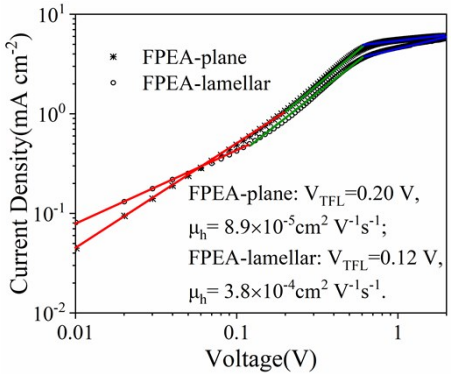

Figure S15 Characteristic J-V curves of hole-only devices.

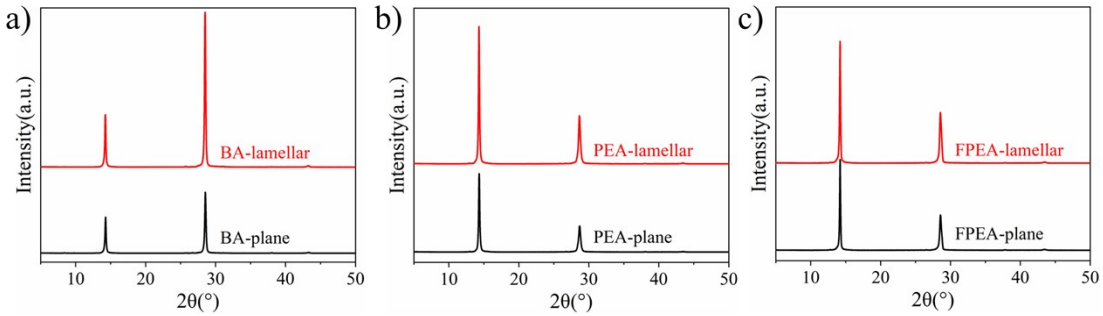

Figure S16 XRD patterns of 2D perovskite films.

Table S7 Full width at half-maximum (FWHM) and intensity ratio of 2D perovskite films.

2D perovskite films	FWHM(14.27°)	FWHM(28.55°)	$I_{(202)}/I_{(111)}$
BA-plane	0.20	0.22	1.85
BA-lamellar	0.19	0.20	3.01
PEA-plane	0.20	0.34	0.56
PEA-lamellar	0.18	0.30	0.60
FPEA-plane	0.17	0.30	0.66
FPEA-lamellar	0.18	0.30	0.70

References

[1] N. Zhou, Y. Shen, L. Li, S. Tan, N. Liu, G. Zheng, Q. Chen and H. Zhou, J Am Chem Soc, 2018, **140**, 459-465.

[2] M. He, J. Liang, Z. Zhang, Y. Qiu, Z. Deng, H. Xu, J. Wang, Y. Yang, Z. Chen and C.-C. Chen, Journal of Materials Chemistry A, 2020, **8**, 25831-25841.

[3] J. Liu, J. Leng, K. Wu, J. Zhang and S. Jin, J Am Chem Soc, 2017, **139**, 1432-1435.